A&A 620, A37 (2018)
https://doi.org/10.1051/0004-6361/201834040


Astronomy & Astrophysics

# NGC 4993 and other short gamma-ray burst host galaxies

## Modelling line and continuum spectra

M. Contini[1,2]

[1] Dipartimento di Fisica e Astronomia "G. Galilei", University of Padova, Vicolo dell'Osservatorio 3, 35122 Padova, Italy
e-mail: contini@post.tau.ac.il
[2] School of Physics and Astronomy, Tel-Aviv University, Tel-Aviv 69978, Israel

Received 8 August 2018 / Accepted 20 September 2018

**ABSTRACT**

We present the spectral detailed modelling of NGC 4993 – the host galaxy of GW 170817 – and other short gamma-ray burst (SGRB) host galaxies. In order to determine their physical conditions and the element abundances, we have gathered spectroscopic and photometric data from the literature. The observation data are sometimes missing, preventing us from fully constraining the model. However, for most of the SGRB hosts the [OIII]5007/H$\beta$ and [NII]6548/H$\alpha$ line ratios are reported. The analysis of NGC 4993 by a composite model (photoionization+shock) confirms that an active galactic nucleus (AGN), most probably a low-ionization nuclear emission-line region (LINER) or a low-luminosity AGN (LLAGN) is the gas photoionization source. Shock velocities and preshock densities are similar to those found in the narrow line region of AGN. O/H and N/H have solar values. For the other SGRB of the sample, we found that O/H ratios are nearly solar, while N/H covers a much larger range of values at redshifts close to 0.4. In NGC 4993, the relative contribution to the spectral energy distribution of an old stellar population, characterized by a blackbody temperature of $T_{bb} = 4000$ K, with respect to bremsstrahlung is higher by a factor of >100 than in most of the local AGN and starburst (SB) galaxies. For the other SGRB that compose the sample, $T_{bb}$ ranges between 2000 K for SGRB 100206A and 8000 K for SGRB 111117A.

**Key words.** radiation mechanisms: general – shock waves – ISM: abundances – galaxies: high-redshift – gamma-ray burst: general – galaxies: active

## 1. Introduction

Gamma-ray bursts (GRB) are short, intense, and isolated flashes (Berger 2013), peaking in the gamma-ray band and occurring at an average rate of one event per day over the whole sky (D'Avanzo 2015) with different spectral and temporal properties. The current scenario in the observation frame distinguishes between GRBs in "short-hard and long-soft" (Berger 2013) bursts. Short duration GRB (SGRB) last less than 2 s, while long GRB (LGRB) have a longer duration (Kouveliotou et al. 1993). Both the localization and detection of afterglows and hosts, and the evidence of lower energy and object number scale suggest (Fox et al. 2005; Barthelmy et al. 2005; Berger et al. 2005) that SGRB are cosmological in origin, with low energetic afterglow, and that their progenitors are not massive stars (Berger 2013). Berger (2009) claims that the association of some SGRB with elliptical galaxies shows that their progenitors belong to an old stellar population, unlike LGRB. However, SGRB hosts have also been found to be star-forming galaxies. The *Niels Gehrels Swift* observatory (hereafter *Swift*; Gehrels et al. 2004) greatly improved the understanding of SGRB progenitors by revealing their location. At present, the majority of SGRB events are typically detected at low $z$, at ∼0.4–0.5 on average (Savaglio et al. 2009; Berger 2014) because of weaker emission at all wavelengths. This is an important issue because it is related to the host galaxy stellar evolution (Contini 2017a). The host galaxy analysis shows that long GRB are found in star-forming galaxies (Fruchter et al. 2006; Savaglio et al. 2009, etc.) while SGRB occur in both star-forming and early type galaxies (D'Avanzo 2015; Bloom et al. 2002; Berger et al. 2005; Fox et al. 2005; Savaglio et al. 2009; Fong et al. 2013). Star formation rates (SFR) in SGRB hosts are low and a broad range of stellar masses is found in agreement with a progenitor old enough to allow neutron star merging (Perley et al. 2012).

The lack of an associated supernova in SGRB and the heterogeneous sample of host galaxies (e.g. Kann 2011) is consistent with a compact binary merger origin (Rosswog & Ramirez-Ruiz 2003), such as neutron stars or black holes. The progenitors were related to an old star population compatible with NS (neutron star) -NS or NS-BH (black hole) encounters (Berger 2009; Eichler et al. 1989). The discovery of GW 170817, which is the neutron star merger directly measured in gravitational waves and associated with an SGRB, allows us to study neutron star mergers in general and to investigate, in particular, whether the gas within NGC 4993, the host galaxy of GW 170817, has particular characteristics (Levan et al. 2017; Villar et al. 2017). Wu et al. (2018) reported on the ensemble of data observed from NGC 4993 from radio to X-ray, which lead to a valid modelling of the continuum spectral energy distribution (SED). Generally, most of the continuum data for GRB host galaxies are available in the infrared (IR) – near optical range. They are explained by models that account for the underlying stellar population flux or fluxes. The large frequency range covered by the dataset used by the aforementioned authors confirms that the photometric fluxes in the IR represent only one of the different contributions to the continuum SED. The most evident ones over a large

frequency range are the radio sources (thermal and synchrotron), dust reprocessed radiation, the underlying stellar emission, and the direct flux from the active sources. They were recognised in local as well as in high $z$ galaxies (e.g. Contini & Contini 2007). However, in some different ranges of the continuum, in particular in the radio and ultraviolet (UV)–X-ray, data are better explained by the bremsstrahlung emitted from the gaseous clouds within the host galaxy, which also emit the spectral lines. The bremsstrahlung is seen over a large frequency range, in particular when shocks are accounted for (Contini 2018). Besides the effect of merging, which affects both high redshift galaxies as well as local ones, shock waves are created by winds, jets, and collisions throughout the galaxies. Therefore shocks should be accounted for by the calculation of line and continuum fluxes. In particular, shocks with velocities >300 km s$^{-1}$ can heat the gas to high temperatures >$10^6$ K, which decrease following the cooling rate downstream. Consequently, the calculated bremsstrahlung can be strong in the X-ray domain and beyond.

In previous papers (e.g. Contini 2016a) we have investigated the physical conditions and the element abundances of GRB host galaxies by the analysis of the observed line spectra at relatively high $z$. We compared them, for example, with those of various supernova (SN) types, AGN, SB, and HII regions. In this paper we investigate line ratios and continuum SED of SGRB host galaxies. The model of the continuum is less constraining than that of the line spectra, therefore we chose our sample SGRB hosts that have reported emission-line fluxes. The sample is somewhat poor in regard to the number of objects. The line spectra suitable to constrain the models generally contain at least H$\beta$, H$\alpha$, [OIII], [OII], and [NII]. The H$\alpha$/H$\beta$ line ratios, which are used to correct for reddening the spectra, cannot be neglected.

Our aim is to determine the physical conditions, the element abundances, and the radiation sources within the NGC 4993 galaxy, which hosts a SGRB, and compare them with other galaxies. Recently NGC 4993 was the site of a gravitational wave (GW) event. NGC 4993 has enough published data to enable line and continuum modelling. For all other SGRB hosts presented in this paper, the continuum SED observations cover only the IR range that corresponds to emission from the underlying stellar population. However, for GRB 050709, GRB 100206A and GRB 130603B the data for the optical-near IR line ratios reported by Berger (2009), Perley et al. (2012), de Ugarte Postigo et al. (2014), Cucchiara et al. (2013), and Soderberg et al. (2006) are enough to constrain the models. The code SUMA (Contini 2018 and references therein; Ferland et al. 1995) calculates the continuum as well as the line fluxes. We show the continuum SED in the diagrams over a large frequency range ($10^8$–$10^{19}$ Hz) even if we did not find any data in the radio, far-IR, optical-UV, and X-ray. The bremsstrahlung results are presented as predictions. For GRB 111117A at $z$ = 2.21 no line fluxes are reported in the literature. Therefore only the old star contribution to the SED is investigated in order to compare it to the SED of other SGRB hosts at lower $z$.

In Sect. 2 the modelling method is applied to NGC 4993 and to other SGRB host galaxies. Discussion and concluding remarks follow in Sect. 3.

## 2. SGRB host spectra

### 2.1. Modelling approach

The code SUMA simulates the physical conditions of an emitting gaseous cloud under the coupled effect of photoionization from a radiation source and shocks assuming a plane-parallel geometry. Two cases are considered relative to cloud propagation: infalling, in which photoionizing radiation reaches the gas on the cloud edge corresponding to the shock front, and ejection, in which the radiation reaches the gas on the edge opposite to the shock front. Calculations and modelling are described in detail by Contini (2018). The main input parameters are those referring to the shock, which are the preshock density $n_0$, the shock velocity $V_s$, the magnetic field $B_0$ (for all galaxy models $B_0 = 10^{-4}$ Gauss is adopted), as well as the source ionizing radiation spectrum and the chemical abundances of He, C, N, O, Ne, Mg, Si, S, Ar, Cl, and Fe, relative to H. The photoionizing radiation adopted for the SB in the GRB host galaxies is a black body (bb). The input parameters are the effective temperature $T_*$ and the ionization parameter $U$. For an AGN, the photoionizing radiation is the power-law radiation flux from the active centre $F$ in number of photons cm$^{-2}$ s$^{-1}$ eV$^{-1}$ at the Lyman limit, and spectral indices $\alpha_{UV} = -1.5$ and $\alpha_X = -0.7$. Generally, $V_s$ is constrained by the full width half maximum (FWHM) of the line profiles and $n_0$ is constrained by the ratio of the characteristic lines. The relative abundances of the elements are constrained by the line ratios. In the case where shock and photoionization act on opposite sides of a plan-parallel nebula, the geometrical width of the nebula, $D$, is an input parameter. The diffuse radiation bridges the two sides, and the smaller the value of $D$, the more entangled are the photoionized and the shocked regions on the opposite sides of the nebula. In this case, a few iterations are necessary to obtain the physical conditions downstream. The effect of dust present in the gas, characterized by the dust-to-gas ratio $d/g$ and the initial grain radius $a_{gr}$ are also consistently taken into account.

The spectra observed from SGRB hosts are often lacking in number of lines. Baldwin, Phillips & Terlevich (BPT) diagrams (Baldwin et al. 1981; Kauffmann 2003; Kewley et al. 2001) for the [OIII]5007/H$\beta$ and [NII]6583/H$\alpha$ line ratios are generally adopted by the community in order to identify the galaxy type in terms of the radiation source. However, extreme physical conditions and relative abundances far from solar, in particular for O/H and N/H, may shift the observed [OIII]/H$\beta$ and [NII]/H$\alpha$ line ratios throughout the BPT diagram towards sectors that were assigned to different galaxy types. For example, a low N/H relative abundance may shift the observed [NII]/H$\alpha$ line ratio emitted from a galaxy towards the SB galaxy domain, although other features of the same object are characteristic of an AGN. This may occur to GRB host galaxies that are located at redshifts higher than local. At high $z$, the over- and under-abundances of the heavy elements are important issues linked with merging, ages and evolution. Therefore, to constrain a model when the line ratios are few we follow a different method. The line ratios of [OIII]5007/H$\beta$ and [NII]6548/H$\alpha$ are generally observed because H$\beta$, H$\alpha$, [OIII], [OII], and [NII] are the strongest lines in the optical range. A first hint towards the choice of the model is obtained by comparing the observed line ratios with the grids of composite models (photoionization+shock) previously calculated (e.g. Contini & Viegas 2001a,b). These models provide an approximate but rich indication of the gas physical conditions calculated within the emitting clouds and of the line and the continuum radiation flux. The line ratios presented by the grids are adapted to HII regions and AGN, respectively. The models (Contini & Viegas 2001a) corresponding to a black-body photoionization flux can be applied to SB galaxies (see Sect. 2). The [OIII]/H$\beta$ and [NII]/H$\alpha$ line ratios alone cannot definitively constrain the model because we deal with two line ratios related to two different elements. Ratios of [OIII] line to Hb flux depend mostly on the ionization parameter and on $V_s$

**Table 1.** Modelling NGC 4993 observed line ratios [OIII]/H$\beta$ = 1.4 and [NII]/H$\alpha$ = 1.26.

| mod | [OIII]/H$\beta$ | [NII]/H$\alpha$ | H$\beta$ | $V_s$ | $n_0$ | $D$ | $T_*$ | $U$ | log$F$ | 12+log(O/H) | 12+log(N/H) |
|---|---|---|---|---|---|---|---|---|---|---|---|
| – | – | – | $a$ | km s$^{-1}$ | cm$^{-3}$ | pc | $10^4$ K | – | $b$ | – | – |
| modSB | 1.41 | 0.13 | 37.7 | 300 | 300 | 1.67 | 5 | 1 | – | 8.82 | 8.0 |
| modSD | 1.4 | 0.146 | 0.0009 | 100 | 100 | 1.9 | – | – | – | 8.82 | 8.0 |
| modAGN1 | 1.43 | 1.26 | 0.05 | 100 | 300 | 1 | – | – | 9.55 | 8.82 | 8.0 |
| modAGN2 | 1.45 | 0.11 | 16.9 | 300 | 300 | 0.27 | – | – | 9.48 | 8.82 | 8.0 |

**Notes.** $^{(a)}$in erg cm$^{-2}$ s$^{-1}$ calculated at the nebula; $^{(b)}F$ is in photons cm$^{-1}$ s$^{-1}$ eV$^{-1}$ at the Lyman limit.

but the [NII]/H$\alpha$ ratios depend strongly on the N/H relative abundances. For example, SN and GRB host N/H ranges between ∼0.1 solar and ∼5 solar (Contini 2017a). We cannot determine a priori whether the best fit to the observed [NII]/H$\alpha$ line ratio could be reached by changing one or more input parameters representing the physical conditions ($V_s$, $n_0$, $D$, $F$ for AGN, $T_*$ and $U$ for SB) or by modifying the N/H relative abundance. The $N^+$ and $H^+$ ions as well as $O^+$ and $H^+$ are correlated by charge exchange reactions, therefore they have a similar trend throughout a cloud. When [OIII]/H$\beta$ and [OII]/H$\beta$ are well reproduced by modelling and solar N/H are adopted, the resulting N/H is calculated by $([NII]/H\beta)_{obs} = ([NII]/H\beta)_{calc}$ $(N/H)/(N/H)_\odot$, where $(N/H)_\odot$ is the solar N/H relative abundance. The [OIII]/H$\beta$ and [OII]/H$\beta$ line ratios are more affected by the physical conditions of the emitting gas than by O/H.

On this basis we calculated a grid of models. We selected the set of models (e.g. Table 1) which best reproduces the line ratios. We obtained the final model by comparing the calculated SED with the observed one. The calculated continuum SED is represented in the diagrams by two lines, one for the bremsstrahlung that covers frequencies from radio to X-ray, and the other for the reprocessed radiation from dust in the IR range. They are calculated by the same model that reproduces the line ratios. In the IR-optical range, the underlying stellar flux emerges from bremsstrahlung and can be blended with dust reradiation when shock velocities are high. The errors in the observed photometric data are <20 percent while the uncertainties in the calculations are <10 percent.

### 2.2. NGC 4993. The host galaxy of GW 170817

We reproduced by detailed modelling the NGC 4993 observed line ratios and the continuum SED (Levan et al. 2017; Palmese et al. 2017; Wu et al. 2018). Observations by Lazer Interferomer Gravitational-Wave Observatory (LIGO)/Virgo scientific collaboration reported gravitational waves that followed the recent neutron star merger event GW 170817. In the frame of our analysis of GRB host line and continuum SED, we calculated the characteristics of the emitting gas from NGC 4993, which is considered to be the host galaxy of GW 170817 at $z$ = 0.009873.

Levan et al. (2017) in their Fig. 4 compared [OIII]/H$\beta$ and [NII]/H$\alpha$ spectroscopic observations with BPT diagnostics. They found that the line ratios fitted the AGN domain. Spectroscopic observations by Palmese et al. (2017, in their Fig. 3 right panel) show [OIII]5007/H$\beta$ and [OII]/H$\alpha$ within the error of Levan et al. (2017) observations. However, Palmese and collaborators admitted that the [OIII]/H$\beta$ line ratio is very uncertain. In Table 1 we report the calculated models that best reproduce the spectroscopic data of Levan et al. (2017). For all of them, O/H solar ($6.6\times10^{-4}$) and N/H solar ($10^{-4}$) are adopted (Grevesse & Sauval 1998). Model modSB is characterized by a bb photoionizing radiation (suitable to SB and HII regions) and relatively high shock velocities ($V_s$ = 300 km s$^{-1}$), and modSD is a shock-dominated model ($F$ = 0 and $U$ = 0) with $V_s$ = 100 km s$^{-1}$. Models modAGN1 and modAGN2 are calculated by a power-law photoionizing flux and different shock velocities, $V_s$ =100 km s$^{-1}$ and $V_s$ = 300 km s$^{-1}$, respectively.

Wu et al. (2018) present new Very Large Array (VLA) and Atacama Large Millimeter/submillimeter Array (ALMA) data and use them for broad-band modelling. The continuum SED is shown in Fig. 1. Haggard et al. (2017) report *Chandra* observations that reveal a compact source consistent with the nucleus of the galaxy and $L_X \sim 2\times10^{39}$ erg s$^{-1}$ (0.5–8 keV). Wu et al. (2018) suggest that the X-ray soft energy excess may indicate thermal emission from a gaseous component in the galaxy. Some observations in the IR were also available (Lambert & Valentijn 1989; De Voucouleurs et al. 1991; Cutri et al. 2003). They were used to constrain the model.

In Figs. 1–4, which account for the continuum SED, each model corresponds to two curves (bremsstrahlung and dust reradiation). The same symbol is used for both. The models that reproduce the SED in Fig. 1 are those used to fit the line ratios in Table 1. Shock velocities of $V_s$ = 300 km s$^{-1}$, which correspond to a maximum temperature downstream of $T \sim 10^6$ K, shift the bremsstrahlung maximum to relatively high frequencies and fit the datum at $7.25\times10^{17}$ Hz (Fig. 1, left diagram), corresponding to soft X-ray. However, the continuum SED in the radio – far IR (FIR) range calculated by models modSB and modAGN2 overpredicts the observed fluxes in the radio range by a factor of approximately ten. Therefore, we dropped modSB and modAGN2. The shock dominated model (modSD) calculated with $V_s$ = 100 km s$^{-1}$ and $n_0$ = 100 cm$^{-3}$ could fit the radio-FIR data adopting a low $d/g = 4\times10^{-5}$. In this case the data in the X-ray have no valid explanation. Moreover, the [NII]/H$\alpha$ ratio is underpredicted by a factor of ten. To adopt a N/H relative abundance ten times solar in order to fit the [NII]/H$\alpha$ ratio is rather an extreme solution. Therefore we selected modAGN1 as the best model at reproducing both the line ratios and the SED of NGC 4993. The model was calculated with $V_s$ = 100 km s$^{-1}$ and $n_0$ = 300 cm$^{-3}$. These shock velocities and densities are found in the narrow line region (NLR) of AGN. The power-law flux is relatively low, suitable to LLAGNs (e.g. Contini 2004) and LINERs.

As already mentioned we calculate the continuum at the nebula whereas the data are observed at Earth. The same is valid for the H$\beta$ line flux. To reduce the calculated H$\beta$ flux by the distance from the galaxy to Earth, we combine the H$\beta$ flux observed at Earth with H$\beta$ calculated at the nebula by $H\beta_{calc} \times r^2 \times ff = H\beta_{obs} \times d^2$. In Table 1 we give $H\beta_{calc}$, while $H\beta_{obs}$ is obtained from the Kennicutt (1998) relation linking SFR with H$\alpha$, adopting H$\alpha$/H$\beta$ = 3 (suitable to calculations accounting for the shocks) and SFR = 0.003 $M_\odot$ yr$^{-1}$ (Pan et al. 2017).

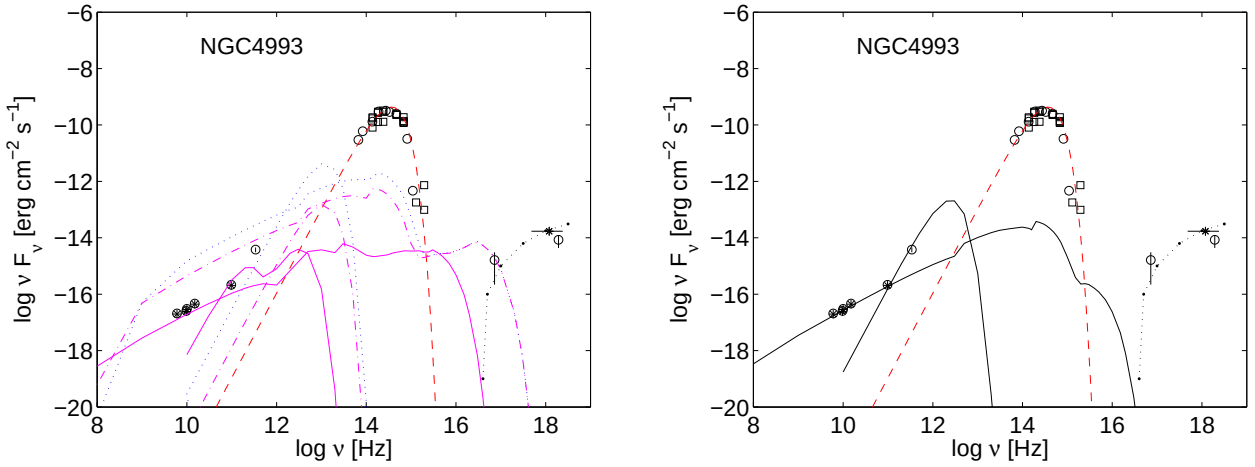


**Fig. 1.** NGC 4993 SED data: Wu et al. (2018; open circles); Levan et al. (2017) (open squares); Blanchard et al. (2017) IR-optical (asterisks): AGN (from NGC 5252) flux in the X-rays (dots). bb flux corresponding to 4000 K (red dashed). *Left*: models modAGN2 (magenta dot-dashed), modSB (blue dotted) and modSD (magenta solid) *Right*: model modAGN1 (black solid); other symbols as in Fig. 1 *left* diagram. Each model is represented by two lines, one is the bremsstrahlung and the other is the dust reprocessed radiation. The models are described in Table 1.

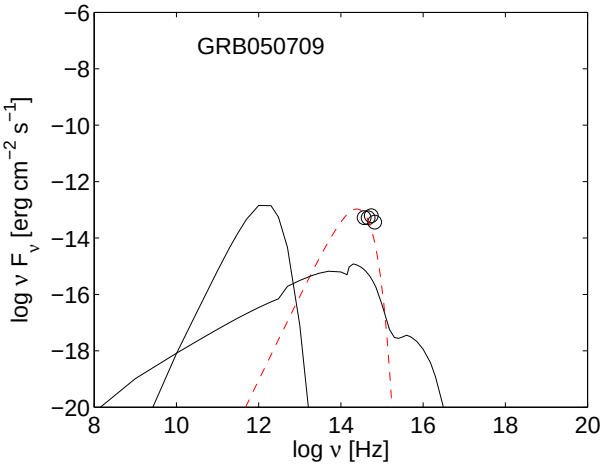


**Fig. 2.** SED of SGRB 050709 host from the Savaglio et al. (2009) sample. Open circles: the data; black solid lines: model modb4 (Table 3); dashed line: bb flux corresponding to $T_{\rm bb} = 3000$ K.

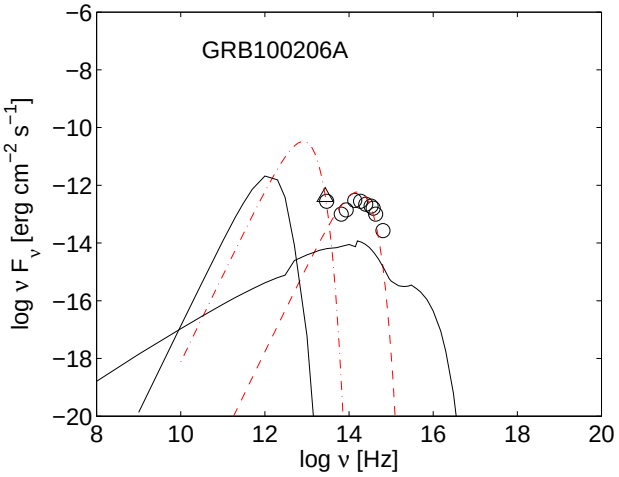


**Fig. 3.** SED of SGRB 100206A host from the Perley et al. (2012) sample. Open circles: the data; black solid lines: model modp1 (Table 5); dashed line: bb flux corresponding to $T_{\rm bb} = 2000$ K; dash-dotted line: bb flux corresponding to $T_{\rm bb} = 100$ K.

Moreover, $ff$ is the filling factor, $r$ the distance of the nebula from the radiation source, and $d$ the distance of the galaxy to Earth. We obtain the factor $f_{\rm s} = (r/d)^2 = {\rm H}\beta_{\rm obs}\ /{\rm H}\beta_{\rm calc}/ff$, which we use in Fig. 1 to shift the calculated continuum SED in order to be compared with the data observed at Earth. In fact we consider that the bremsstrahlung is emitted from the same cloud that emits the lines (e.g. H$\beta$). From Fig. 1 (right diagram) the best fit in the radio – near IR (NIR) range is obtained by $\log(f_{\rm s}) = -11.7$, while $\log({\rm H}\beta_{\rm obs}/{\rm H}\beta_{\rm calc}) = -14$. Then we obtain $ff = 0.005$. Using the distance from Earth $d = 42.9$ Mpc, $r$ is 60 pc. To reproduce the dust reradiation bump in Fig. 1 right, we adopted $d/g = 0.008$ and $a_{gr} = 0.1\,\mu$m.

Considering that an AGN is present in the NGC 4993 galaxy, we tried to fit the X-ray data presented by Wu et al. (2018) by the (absorbed) power-law model, which was successfully adopted to reproduce the X-ray flux at high frequencies observed for other AGN such as the Circinus galaxy (Contini et al. 1998a) and NGC 5252 (Contini et al. 1998b). The observed X-ray flux from the NGC 4993 AGN nucleus is relatively low, exceeding the maximum radio flux by a factor of ∼100 (Fig. 1 right), while for example in the Circinus AGN this factor is $>10^5$ and in NGC 5252 it is ≥1000. Wu et al. (2018) claim that this X-ray emission is mostly due to a weak LLAGN. The results agree with Palmese et al. (2017) who believe that the stellar model fit to NGC 4993 reveals the existence of weak ionized gas emission while the line ratios are most probably produced by a harder ionizing source than star formation lying in the AGN region of the Baldwin et al. (1981) diagram. Blanchard et al. (2017) argue that there is a weak AGN present in the core of the galaxy on the basis of radio and X-ray emission, in agreement with Wu et al. (2018) who suggest a LLAGN or even some sort of shock. Palmese et al. (2017) concluded that there is no evidence of recent star-formation from the spectrum, irrespective of the uncertain [OIII]/H$\beta$. From the Balmer decrement they found $E(B-V) = 0.12 \pm 0.50$. Dust obscuration does not play a role in SFR estimation calculated on the basis of the H$\alpha$ luminosity.

In summary, the observed SED presented by Wu et al. (2018) shows soft and hard X-ray emission at $\log(\nu[{\rm Herz}]) \geq 17.8$. Our modelling confirms that velocities throughout NGC 4993 are ∼100 km s$^{-1}$. Therefore, both soft and hard X-rays (Fig. 1, left diagram) come from the AGN radiation. On the other

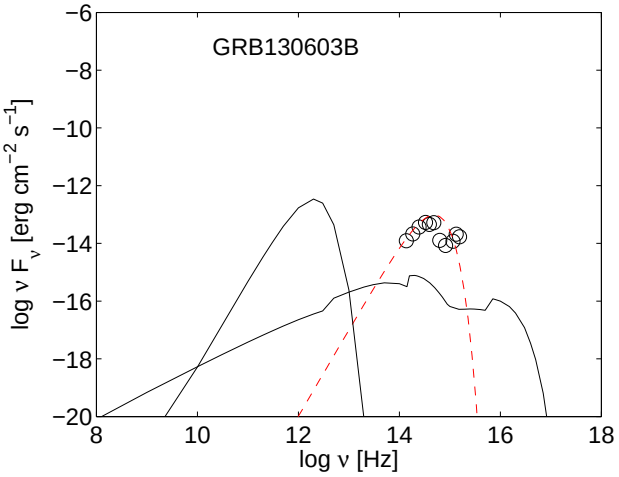


**Fig. 4.** SED of GRB 130603B host from the de Ugarte Postigo et al. (2014) sample. Open circles: the data; black solid lines: model MS5 (Table 6); dashed line: bb flux corresponding to $T_{bb} = 6000$ K.

hand, comparison with the SED calculated with $V_s \geq 300$ km s$^{-1}$ could nicely fit NGC 4993 data in the soft X-rays domain. However, this model is dismissed because it overpredicts the observed fluxes in the radio range. Moreover, it corresponds to [NII]/H$\alpha = 0.16$. Figure 1 shows that bb radiation flux from the underlying population stars corresponding to $T_{bb} = 4000$ K is high relative to bremsstrahlung.

As Palmese and collaborators concluded, NGC 4993 experienced a minor galaxy merger with signs that are still evident. The spectral analysis shows AGN activity and an old stellar population. In the IR-optical domain the bb radiation corresponding to the old underlying star population at 4000 K reproduces the data satisfactorily. Compared to local SB and AGN galaxies (Contini & Contini 2007), the bb flux-to-bremsstrahlung ratio of >100 for old stars in the IR-optical frequency range is remarkably high.

### *2.3. Other SGRB host galaxies*

#### 2.3.1. Berger (2009) sample

We present modelling results of the line spectra observed from the host galaxies included in the Berger (2009) SGRB sample. The calculated continuum is compared to the SED observed by Savaglio et al. (2009) in the IR for SGRB 050709.

The Berger sample of SGRB hosts is relatively poor in number of objects. In Table 2 we present the observed SGRB host galaxy line fluxes. The observed line ratios to H$\beta$ (in the underlying row) for each object are followed in the next row by the calculated ones. The models, represented by the set of the main input parameters that lead to the best fit, are shown in Table 3. In the last column of Table 3 the metallicities evaluated by Berger (2009) are shown. The lines are observed at Earth but calculated at the emitting nebula. We compared the calculated ratios of line to H$\beta$ fluxes to the observed ones (which were corrected for reddening). For SGRB 061006 and SGRB 070724, H$\alpha$ and [NII] line fluxes are lacking and the ratios of line to H$\beta$ fluxes were modelled directly without reddening correction. The [OII] 3727+ doublet, which is close to the near UV domain, is more affected by correction than the other observed lines in the optical–IR. Nevertheless, the values of the input parameters that were adopted by the model should be taken with caution. GRB 51221a is shown in Sect. 2.3.4. When Berger (2009) analysed the spectra by the strong line methods, he found that short GRB host luminosities are systematically brighter than those of long GRB in the same redshift range. Berger obtained luminosities $L_B \sim 0.1$–$1.5\,L_\odot$, SFR $\sim 0.2$–$6\,M_\odot$ yr$^{-1}$, and metallicities 12+log(O/H) $\sim 8.5$–$8.9$ ($3.2\times10^{-4}$ and $7.9\times10^{-4}$, respectively) higher than for LGRBs. Specific SFR for SGRB have a median value lower than for LGRB SFR hosts. Comparing the results obtained for the Niino et al. (2017) sample of LGRB hosts (Contini 2017b) to the present ones in Tables 3 and 5, we obtain similar results.

We have selected SGRB 050709 and SGRB 050724 photometric data from the Savaglio et al. (2009) sample to model the SED. They show at least three datapoints. However, for SGRB 050724 we could not find any of the observed line ratios generally used to model the host galaxy. For SGRB 050709 we calculated the continuum SED by model modb4 (Table 3) at the nebula. Data from Savaglio et al. (2009) for SGRB 050709 are reproduced by a stellar bb at $T_{bb} = 3000$ K in Fig. 2. Proceeding as for NGC 4993 (Sect. 3), we combined H$\beta_{calc}$ (Table 3) with H$\beta_{obs}$ presented by Berger (2009) in his Table 2. Adopting $ff = 0.01$ we calculated $f_s$ and accordingly we shifted the calculated continuum in Fig. 2. Hopefully future data will confirm the modelling. The distance of the emitting nebula from the photoionizing source $r$ is 144 pc.

#### 2.3.2. SGRB 100206A host by Perley et al. (2012)

Perley et al. (2012) presented data from *Swift* for GRB 1002016A, a disk galaxy at $z = 0.4068$ that is rapidly forming stars. The galaxy is red, obscured and the interpretation of the spectra reported by the aforementioned authors leads to a high metallicity (12+log(O/H) = 9.2). They also explain the SED by a substantial stellar mass of older stars although the IR luminosity ($4\times10^{11}\,L_\odot$) could indicate young star formation. Perley et al. (2012) in their Tables 2 and 4 presented the spectra of two galaxies (G1 and G2) near the X-ray telescope (XRT) error circle, which were considered as possible host galaxies. The data were acquired by the Low Resolution Imaging Spectrograph (LRIS) on the KeckI 10m telescope. In Table 4 we only examine galaxy G1 line ratios by detailed modelling because G2 data are too few to constrain the model. Moreover, Perley and collaborators decomposed G1 into three semi-distinct clumps. Their aim was to determine metallicities (in terms of O/H). In Table 5, we present the model results calculated from the spectra presented by Perley et al. (2012) for galaxy G1 and for the different clumps. Unfortunately the lines are few, nevertheless they are the minimum required to constrain the models. Our results show relatively high preshock densities in the emitting clouds, which are more extended than those in LGRB hosts (Contini 2017a). We find solar O/H (12+log(O/H) = 8.82) in nearly all the observed positions, while N/H are higher than solar by a small factor (<2), but higher by a factor of approximately ten than for the SGRB hosts in the Berger sample. The N/O ratios are the highest ever calculated for SGRB, even higher than those calculated for the de Ugarte Postigo et al. (2014) GRB spectra and those calculated for long GRB at the same redshift. The underlying stellar contribution to the SED corresponds to $T_{bb} = 2000$ K. The calculated SED is shown in Fig. 3.

#### 2.3.3. SGRB 130603B (de Ugarte Postigo et al. 2014)

SGRB 130603B has been observed in the IR enabling the modelling of the SED.

**Table 2.** Modelling Berger (2009) SGRB spectra.

| GRB | $z$ | [OII] 3727 | H$\beta$ 4865 | [OIII] 5007+ | H$\alpha$ 6563 | [NII] 6548+ | Ref. |
|---|---|---|---|---|---|---|---|
| 061006[a] | 0.4377 | 4.1 | 0.9 | 1.5 | – | – | Berger (2009) |
| 061006[b] | | 4.24 | 1 | 1.89 | – | – | |
| modb1 | | 4.5 | 1 | 1.86 | – | – | |
| 061210[a] | 0.4095 | 22. | 7.6 | 10.5 | 11. | 2.4 | Berger (2009) |
| 061210[c] | | 1.71 | 1 | 1.6 | 3 | 0.15 | |
| modb2 | | 1.77 | 1 | 1.57 | 2.98 | 0.15 | |
| 070724[a] | 0.4571 | 37. | 15. | 17. | – | – | Berger (2009) |
| 070724[b] | | 2.47 | 1 | 1.13 | – | – | |
| modb3 | | 2.54 | 1 | 1.18 | – | – | |
| 050709[a] | 0.1606 | – | 6.6 | 26 | 26 | 1.8 | Fox et al. (2005) |
| 050709[c] | | – | 1 | 3.7 | 3 | 0.29 | |
| modb4 | | (1.69) | 1 | 3.78 | 3 | 0.29 | |

**Notes.** [(a)]Line flux in $10^{-17}$ erg cm$^{-2}$ s$^{-1}$ observed at Earth; [(b)]line ratios to H$\beta$; [(c)]corrected line ratios to H$\beta$.

**Table 3.** Models for Berger (2009) SGRB spectra.

| mod | $V_s$ km s$^{-1}$ | $n_0$ cm$^{-3}$ | $D$ $10^{18}$ cm | 12+log(N/H) | 12+log(O/H) | $T_*$ $10^4$ K | $U$ – | H$\beta$ $a$ | 12+log(O/H)(Berger) |
|---|---|---|---|---|---|---|---|---|---|
| modb1 | 100 | 100 | 0.8 | 7. | 8.82 | 5.7 | 0.005 | 0.006 | 8.63 |
| modb2 | 100 | 300 | 2.8 | 6.9 | 8.8 | 4.3 | 0.03 | 0.167 | 8.82 |
| modb3 | 120 | 250 | 3 | – | 8.81 | 4.9 | 0.013 | 0.072 | 8.88 |
| modb4 | 120 | 250 | 3 | 7.25 | 8.81 | 4.8 | 0.06 | 0.19 | 8.50 |

**Notes.** [(a)]In erg cm$^{-2}$ s$^{-1}$ calculated at the nebula.

**Table 4.** Modelling Perley et al. (2012) short GRB 100206A host spectra at $z = 0.4068$.

| | [OII] 3727 | H$\beta$ 4865 | [OIII] 5007+ | H$\alpha$ 6563 | [NII] 6548+ | [SII] 6716 | [SII] 6731 |
|---|---|---|---|---|---|---|---|
| subtr[a] | $19.6 \pm 2.1$ | $21.8 \pm 1.9$ | $6.8 \pm 1.6$ | $112.8 \pm 1.6$ | $58.8 \pm 2.5$ | $20.4 \pm 3.1$ | $13.6 \pm 1.7$ |
| F/H$\beta$ | 0.9 | 1 | 0.31 | 5.17 | 2.7 | 0.93 | 0.62 |
| corr | 1.34 | 1 | 0.23 | 3 | 1.58 | 0.53 | 0.35 |
| modp1 | 1.6 | 1 | 0.23 | 3 | 1.54 | 0.43 | 0.35 |
| North (subtr)[a] | $7.91 \pm 1.55$ | $9.59 \pm 1.35$ | $1.22 \pm 0.74$ | $33.41 \pm 1.08$ | $16.98 \pm 1.54$ | $4.44 \pm 1.73$ | $4.0 \pm 1.61$ |
| F/H$\beta$ | 0.82 | 1 | 0.127 | 3.48 | 1.77 | 0.46 | 0.42 |
| modp2 | 0.82 | 1 | 0.127 | 3.12 | 1.6 | 0.4 | 0.42 |
| Center (subtr)[a] | $5.69 \pm 1.40$ | $7.57 \pm 1.24$ | $3.5 \pm 1.28$ | $60.55 \pm 1.32$ | $33.9 \pm 2$ | $3.33 \pm 2.50$ | $3.24 \pm 2.19$ |
| F/H$\beta$ | 0.75 | 1 | 0.46 | 8. | 4.47 | 0.44 | 0.43 |
| corr | 1.57 | 1 | 0.27 | 3 | 1.67 | 0.15 | 0.149 |
| modp3 | 1.64 | 1 | 0.28 | 3.2 | 1.4 | 0.14 | 0.14 |
| South (subtr)[a] | $4.02 \pm 1.23$ | $3.61 \pm 1.02$ | $1.68 \pm 0.70$ | $17.7 \pm 0.83$ | $10.54 \pm 1.33$ | $3.06 \pm 1.09$ | $4.94 \pm 1.27$ |
| F/H$\beta$ | 1.11 | 1 | 0.465 | 4.9 | 2.92 | 0.85 | 1.37 |
| corr | 1.6 | 1 | 0.36 | 3 | 1.8 | 0.5 | 0.81 |
| modp4 | 1.57 | 1 | 0.367 | 3.2 | 1.8 | 0.51 | 0.61 |

**Notes.** [(a)]In $10^{-17}$ erg cm$^{-2}$ s$^{-1}$.

We report in the following the modelling of SGRB 130603B line ratios (Table 6) by Contini (2016a) and in Fig. 4 the modelling of the SED. The spectra by FOcal Reducer and low dispersion (FORS2) at the Very Large Telescope (VLT) and the Ohio State InfraRed Imager/Spectrometer (OSIRIS) at Gran Telescopio Canarias (GTC) were observed by de Ugarte Postigo et al. (2014). They suggested that SGRB derive from the merger of compact objects, in particular SGRB 130603B, on the basis of the detection of "kilonova"-like signatures associated with *Swift*. The host galaxy is a perturbed spiral due to interaction with another galaxy. In the spectrum taken by X-shooter, the afterglow dominates the continuum but the lines are emitted from the host, therefore they are used for modelling. FORS spectra show the core, the arm, and the opposite side of the galaxy. The GRB is located on the outskirts of the galaxy in a tidally disrupted arm at ~5.4 kpc from the brightest point of the host. The host was covered by two slit positions along the major axis and two spectra were taken at

**Table 5.** Models for Perley et al. (2012) GRB 100206A spectra.

| | $V_s$ km s$^{-1}$ | $n_0$ cm$^{-3}$ | $D$ $10^{18}$ cm | 12+log(N/H) | 12+log(O/H) | 12+log(S/H) | $T_*$ $10^4$ K | $U$ 0.001 | H$\beta$ $a$ |
|---|---|---|---|---|---|---|---|---|---|
| modp1 | 100 | 120 | 4.9 | 8.04 | 8.78 | 6.48 | 4.4 | 0.9 | 0.003 |
| modp2 | 100 | 250 | 3.3 | 8.25 | 8.82 | 6.95 | 3.6 | 0.6 | 0.025 |
| modp3 | 100 | 200 | 3.3 | 8.04 | 8.82 | 6.40 | 4.6 | 0.6 | 0.0098 |
| modp4 | 120 | 200 | 1.9 | 8.15 | 8.82 | 7.11 | 4 | 0.6 | 0.0092 |

**Notes.** [(a)]In erg cm$^{-2}$ s$^{-1}$ calculated at the nebula.

**Table 6.** Models for SGRB 130603B at $z = 0.356$ and SGRB 051221a at $z = 0.546$ host galaxy spectra.

| | OT site[a] | mS1 | OT site[b] | mS2 | core[b] | mS3 | arm[b] | mS4 | obs[c] | mS5 | 051221a[d] | mS6 |
|---|---|---|---|---|---|---|---|---|---|---|---|---|
| [OII]3727+ | 4.47 | 4.5 | 3.4 | 3.6 | 3.55 | 3.7 | 4.3 | 4.3 | 3.05 | 3.2 | 7.8 | 7.5 |
| H$\gamma$ | – | 0.46 | 0.89 | 0.49 | 0.49 | 0.46 | [0.5] | 0.46 | – | 0.46 | 0.46 | 0.46 |
| H$\beta$ | 1 | 1 | 1 | 1 | 1 | 1 | 1 | 1 | 1 | 1 | 1 | 1 |
| [OIII[5007+ | 0.87 | 0.9 | 0.76 | 0.8 | 0.75 | 0.8 | 0.85 | 0.85 | 0.77 | 0.7 | 5.17 | 5.15 |
| H$\alpha$ | 3 | 3 | 3 | 2.96 | 3 | 2.96 | 3 | 3 | 3 | 3 | – | 3 |
| [NII]6585 | 0.7 | 0.76 | 0.57 | 0.56 | 0.85 | 0.85 | 1.8 | 1.8 | 0.78 | 0.8 | – | – |
| [SII]6717 | 0.66 | 0.7 | 1.19 | 1.1 | 0.63 | 0.66 | 0.27 | 0.5 | – | – | – | – |
| [SII]6731 | 0.33 | 0.6 | 0.56 | 0.97 | 0.5 | 0.59 | 0.5 | 0.45 | – | – | – | – |
| $V_s$(km s$^{-1}$) | – | 140 | – | 150 | – | 150 | – | 140 | – | 120 | – | 150 |
| $n_0$ (cm$^{-3}$) | – | 120 | – | 130 | – | 130 | – | 120 | – | 100 | – | 100 |
| $B_0$ ($10^{-4}$ G) | – | 3 | – | 3 | – | 3 | – | 3 | – | 2 | – | 1 |
| $D^e$ | – | 5.3 | – | 1 | – | 1 | – | 1 | – | 3 | – | 0.2 |
| 12+log(O/H) | – | 8.82 | – | 8.8 | – | 8.8 | – | 8.82 | – | 8.81 | – | 8.82 |
| 12+log(N/H) | – | 7.3 | – | 7.3 | – | 7.48 | – | 7.8 | – | 7.48 | – | 7.11 |
| 12+log(S/H) | – | 6.6 | – | 7.0 | – | 6.78 | – | 6.48 | – | 6.48 | – | 6.48 |
| $T_*$($10^4$ K) | – | 3.6 | – | 3.5 | – | 3.5 | – | 3.6 | – | 3.8 | – | 8.3 |
| $U$ | – | 0.014 | – | 0.01 | – | 0.01 | – | 0.014 | – | 0.007 | – | 0.007 |
| H$\beta^f$ | – | 0.014 | – | 0.016 | – | 0.016 | – | 0.03 | – | 0.014 | – | 0.007 |
| 12+log(O/H)[g] | – | 7.94-8.98 | - | 8.16–8.88 | – | 8.17–8.87 | – | 8.26–8.77 | – | 8.5 | – | 8.7 |

**Notes.** [(a)]de Ugarte Postigo et al. (2014) (X-shooter); [(b)]de Ugarte Postigo et al. (2014) (FORS); [(c)]Cucchiara et al. (2013) (DEIMOS); [(d)]Soderberg et al. (2006) (Gemini-N GMOS); [(e)]in $10^{18}$ cm; [(f)]in erg cm$^{-2}$ s$^{-1}$; [(g)]evaluated by the observers adopting the strong line method.

different times plus an X-shooter spectrum covering the afterglow position.

The results of modelling the X-shooter and FORS reddening-corrected spectra observed at VLT by de Ugarte Postigo and collaborators (see Contini 2016a in their Table 12) are reported in Table 6, neglecting the GTC spectra, which do not include the H$\alpha$ line. Line fluxes and uncertainties before correction are given by de Ugarte Postigo et al. (2014). The spectrum observed by Cucchiara et al. (2013) for SGRB 130603B is also shown for comparison. Most of the spectra presented by SGRB surveys (e.g. Fong et al. 2013), do not contain enough lines to constrain the models. In Table 6 each spectrum is followed in the next column by the model (mS1–mS6) that best reproduces the line ratios. The parameters representing the physical conditions and the relative abundances are reported at the bottom of the table. To best reproduce all the line ratios presented in Table 6, S/H relative abundances lower than solar ($(S/H)_\odot = 1.6 \times 10^{-5}$, Grevesse & Sauval 1998) by factors ≥2 were adopted. S/H in FORS optical transient (OT) site is near solar. The cloud's geometrical thickness is relatively large ($D = 1.8$ pc) from the modelling of the X-shooter (OT site) results, whereas $D = 3$ pc is used to fit the FORS spectra, showing a larger cloud fragmentation. The spectrum reported by Cucchiara et al. (2013) is reproduced by a model (mS5) similar to those used to fit the spectra observed by de Ugarte Postigo and collaborators. The SB temperatures and ionization parameters that result from modelling the host spectra are relatively low ($T_* \sim 3.5 \times 10^4$ K and $U \sim 0.01$). The continuum SED of SGRB 130603B (de Ugarte Postigo et al. 2014) appears in Fig. 4. The underlying stellar contribution to SGRB 130603B corresponds to $T_* = 6000$ K.

### 2.3.4. SGRB 051221a (Soderberg et al. 2006)

The spectrum observed by Soderberg et al. (2006) for SGRB 051221a at $z = 0.546$ and the relative model mS6 are reported from Contini (2016a, in their Table 12, last two columns) in Table 6. The line ratios were reddening-corrected, adopting H$\gamma$/H$\beta = 0.46$. The best-fitting model shows 12+log(O/H) = 8.8, in agreement with Soderberg et al. (2006) who obtained 8.7 by the R32 method (upper branch). We have found $T_* = 8.2 \times 10^4$ K and $U = 0.007$. The star effective temperature is higher than for SGRB 130603B, where $T_* \sim 3.5 \times 10^4$ K. The ionization parameter, however, is similar. Low ionization parameters (i.e. the number of photons reaching the nebula per number of electrons at the nebula) roughly indicate that the host's observed positions are far from the star-forming region or that the photon flux is prevented from reaching the nebula. The hosts show N/H ≤ 0.5 solar and O/H solar. For SGRB 051221a the photometric data are too few to be used to model the SED.

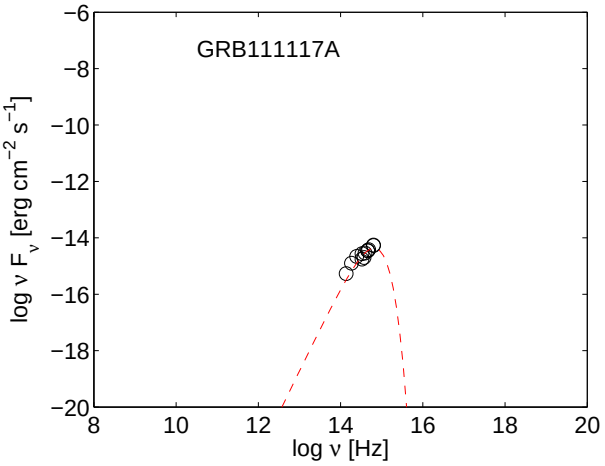


**Fig. 5.** SED of GRB 111117A host from Selsing et al. (2018). Open circles: the data; dashed line: bb flux corresponding to $T_{\rm bb} = 8000$ K.

#### 2.3.5. GRB 111117A host SED (Selsing et al. 2018)

Selsing et al. (2018) presented spectroscopy and photometry data of the GRB 111117A host galaxy with an estimated redshift of $z = 2.211$. The galaxy is actively forming stars. At $z = 2.211$ GRB 111117A is the most distant high-confidence SGRB detected to date. Spectroscopic observations used VLT/X-shooter (Vernet et al. 2011) at four separate epochs. The burst was observed 38 h after the burst alert telescope (BAT) trigger. Selsing and collaborators determined the redshift value from the simultaneous detection of emission lines belonging to Ly$\alpha$, [OII]3727, [OIII]5007 and H$\alpha$, but H$\beta$ was detected at low significance. They used $F_{\rm H\alpha} = 4.1 \times 10^{-17}$ erg cm$^{-2}$ s$^{-1}$ to calculate the SFR $= 18 \pm 3\ M_\odot$ yr$^{-1}$. No dust was deduced from the Ly$\alpha$, so the spectra were not reddening corrected. The photometric data of the aforementioned authors appear in Fig. 5. They are reproduced by a bb flux corresponding to $T_{\rm bb} = 8000$ K, in agreement with Margutti et al. (2012) who reported that GRB 111117A has a young age and vigorous star formation.

## 3. Discussion and concluding remarks

In this work we have presented the analysis of line and continuum spectra of NGC 4993 and of a few SGRB host galaxies by exploiting the spectroscopic and photometric data available in the literature. For some objects included in our sample, the spectra show the [OIII]/H$\beta$ and [NII]/H$\alpha$ line ratios. The diagnostics (e.g. Baldwin et al. 1981; Kewley et al. 2001) are generally used to recognise the type of flux that photoionizes the GRB host gas (a black body for SBs and HII regions, or a power-law for AGNs). The literature data are sometimes lacking and have not always allowed us to constrain the analysis results. We have nevertheless managed to obtain a more complete picture of the gas physical conditions (i.e. shock velocity, preshock density, geometrical thickness of the emitting clouds, flux intensity from the AGN or from the SB, SB effective temperature, and ionization parameter) and chemical abundances by the detailed modelling of other line ratios (e.g. [OII]3727+/H$\beta$, [SII]6717/[SII]6731).

We have investigated in particular NGC 4993, the host galaxy of GW 170817. The results confirm that an AGN, such as an LLAGN or a LINER, must be the source of gas photoionization. NGC 4993 was formerly identified as an LLAGN on the basis of the BTP diagrams. Shock velocities (~100 km s$^{-1}$) and preshock densities (~300 cm$^{-3}$), constrained by the simultaneous and consistent fit of the line ratios and of the SED, are similar to those found in the AGN narrow line ragion, O/H and N/H relative abundances are solar. The ensemble of data reported by Wu et al. (2018) for the NGC 4993 continuum ranges from radio to X-ray. By modelling the continuum SED we have found that the contribution of an old, underlying stellar population with $T_{\rm bb} = 4000$ K is very high relative to the bremsstrahlung in the near IR range and higher by a factor >100 than for local AGN and SB galaxies. Radiation in the radio is thermal bremsstrahlung, while in both soft and hard X-ray it comes from the AGN. For the other SGRB hosts, most of the datasets for the GRB host galaxy continuum are available in the IR-near optical range and are explained by models that account for the underlying stellar flux. We found $T_{\rm bb}$ between 2000 K for SGRB 1002016A and 8000 K for SGRB 111117A.

On the basis of the results obtained for NGC 4993, for LGRB hosts (Contini 2018) and for different types of local galaxies (e.g. AGN, SB Contini & Contini 2007) we suggest that bremsstrahlung from the clouds that emit the line spectra could

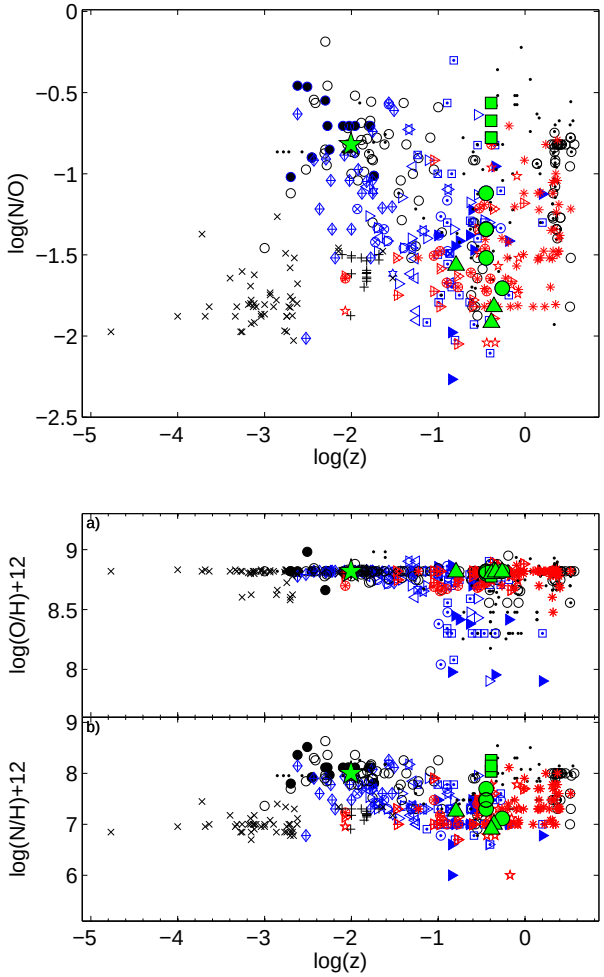


**Fig. 6.** *Top*: distribution of N/O calculated by detailed modelling for SGRB hosts as function of the redshift. Large green circles: from the spectra observed by de Ugarte Postigo et al. (2014). Large green squares: from Perley et al. (2012). Large green triangles: from Berger. Large green star: NGC 4993. The results obtained in the present paper are superimposed on those calculated for SN host galaxies, long GRB hosts, short GRB hosts, SB, AGN, and LINERs (both local and at higher $z$), low-luminosity nearby galaxies, and HII regions in local galaxies. Symbols are explained in Table 8. *Bottom*: the same for O/H and N/H relative abundances. Symbols as in the top diagram.

**Table 7.** Results of detailed modelling calculations.

| SGRB | $V_s$ km s$^{-1}$ | $n_0$ cm$^{-3}$ | $D$ pc | 12+log(N/H) – | 12+log(O/H) – | $T_*$ $10^4$ K | $U$ – | log($F$) $a$ | H$\beta$ $b$ | $T_{bb}$ K | $z$ |
|---|---|---|---|---|---|---|---|---|---|---|---|
| NGC 4993 | 100 | 300 | 0.3 | 8. | 8.82 | – | – | 9.55 | 0.05 | 4000 | 0.009873 |
| 050709 | 120 | 250 | 1 | 7.25 | 8.81 | 4.8 | 0.06 | – | 0.19 | 3000 | 0.167 |
| 051221a | 150 | 100 | 0.07 | 7.11 | 8.82 | 8.3 | 0.007 | – | 0.007 | – | 0.546 |
| 061006 | 100 | 100 | 0.27 | 7.0 | 8.82 | 5.7 | 0.05 | – | 0.006 | – | 0.4377 |
| 061210 | 100 | 300 | 0.93 | 6.9 | 8.80 | 4.3 | 0.03 | – | 0.167 | – | 0.4095 |
| 070724 | 120 | 250 | 1 | 7.25 | 8.81 | 4.9 | 0.013 | – | 0.072 | – | 0.4571 |
| 100206A | 100 | 120 | 1.7 | 8.04 | 8.78 | 4.4 | 0.9 | – | 0.003 | 2000 | 0.4068 |
| 100206A N | 100 | 250 | 1.1 | 8.25 | 8.82 | 3.6 | 0.6 | – | 0.025 | – | |
| 100206A C | 100 | 200 | 1.1 | 8.04 | 8.82 | 4.6 | 0.6 | – | 0.0098 | – | |
| 100206A S | 120 | 200 | 0.7 | 8.15 | 8.82 | 4 | 0.6 | – | 0.0092 | – | |
| 130603B OT[c] | 140 | 120 | 1.8 | 7.30 | 8.82 | 3.6 | 0.014 | – | 0.014 | 6000 | 0.356 |
| 130603B OT[d] | 150 | 130 | 0.3 | 7.30 | 8.80 | 3.5 | 0.01 | – | 0.016 | – | |
| 130603B core | 150 | 130 | 0.3 | 7.48 | 8.80 | 3.5 | 0.01 | – | 0.016 | – | |
| 130603B arm | 140 | 120 | 0.3 | 7.7 | 8.82 | 3.6 | 0.014 | – | 0.03 | – | |
| 130603B[e] | 120 | 100 | 1 | 7.47 | 8.813 | 3.8 | 0.007 | – | 0.014 | – | |

**Notes.** [(a)] $F$ is in photon cm$^{-2}$ s$^{-1}$ eV$^{-1}$ at the Lyman limit; [(b)] in erg cm$^{-2}$ s$^{-1}$ calculated at the nebula; [(c)] X- shooter; [(d)] FORS; [(e)] DEIMOS.

**Table 8.** Symbols in Fig. 6.

| Symbol | Object | Ref. |
|---|---|---|
| Encircled dot | SLSNR hosts | (1) |
| Triangles at $z \geq 0.1$ | SLSNII hosts | (2) |
| Filled triangles | SLSNI hosts | (3) |
| Square+dot | SD models for SLSN hosts | (4) |
| Square+cross | Type Ic host central | (5) |
| Circle+cross | Type Ic host at SN positions | (6) |
| Triangles at $z \leq 0.1$ | SN Ib host | (7) |
| Encircled triangles | SN IIb hosts | (8) |
| Opposite triangles | SN Ic hosts | (9) |
| Double triangles | SN IcBL hosts | (10) |
| Hexagrams | SN Ibc | (11) |
| Asterisks | GRB hosts | (12) |
| Triangle+cross | LGRB hosts | (13) |
| Pentagrams | LGRB different hosts | (14) |
| Triangle+plus | LGRB hosts with WR stars | (15) |
| Encircled asterisks | LGRB at lo $z$ | (16) |
| Hexagrams (green) | SGRB hosts | (17) |
| Diamonds | Other galaxies | (18) |
| Dots | Starburst galaxies | (19,25) |
| Circles | AGN | (20,21,25) |
| Filled circles | LINER | (22) |
| Plus | Low-luminosity nearby galaxies | (23) |
| Cross | HII regions in local galaxies | (24) |
| Diamonds+plus | TypeI SN hosts | (26) |

**References.** (1), (2), (3), (4) (Leloudas et al. 2015); (5), (6) (Modjaz et al. 2008); (7), (8), (9), (10), (11) (Sanders et al. 2012); (12) (Krühler et al. 2015); (13) (Savaglio et al. 2009); (14) (Contini 2016a, Table 8); (15) (Han et al. 2010); (16) (Niino et al. 2017); (17) (de Ugarte Postigo et al. 2014); (18), (19), (20) (Contini 2014; and references therein); (21) (Koski 1978; Cohen 1983; Kraemer et al. 1994; Dopita et al. 2015); (22) (Contini 1997); (23) (Marino et al. 2013); (24) (Berg et al. 2012); (25) (Contini 2016b); (26) (Gallagher et al. 2005).

also be the main contributor to the continuum in the radio, optical, UV, and soft X-ray range of SGRB hosts, while the underlying stellar bb radiation in the IR-optical domain is constrained by photometric observations in the infrared. Moreover, dust-reprocessed radiation in the IR range (consistently calculated with the gas bremsstrahlung) and the flux from the photoionising source in the X-ray also shape the continuum SED. The results calculated for the SGRB hosts are summarized in Table 7.

In the diagrams in Fig. 6 we have added the N/O relative abundances calculated for the SGRB hosts as a function of the redshift to those presented for LGRB hosts, SN hosts of many types, HII regions, AGN, LINER, and SB galaxies (Contini 2016a). Symbols are described in Table 8. The bottom diagrams show the results for O/H and N/H relative abundances as a function of $z$. It is evident that O/H is about constant at the solar value, while N/O covers a large range of values determined by the N/H ratios ($6.8 \leq \log(\mathrm{N/H})+12 \leq 8.25$) over a small redshift range centred around $z \sim 0.4$. At present, only limited data at other $z$ are available. N/O abundance ratios calculated along different positions in GRB 100206B – observed by Perley et al. (2012) – reach the maximum values calculated for LGRB hosts at higher redshifts. In Fig. 6 most of the SGRB hosts are located at the confluence (at $z$ close to 0.4) of the N/O decreasing slope with decreasing $z$ of GRB hosts and of the increasing N/O slope with decreasing $z$ of SN hosts at lower $z$. These trends can be explained by considering that intermediate-mass stars between 4 and 8 $M_\odot$dominate nitrogen production, which is primary at low metallicities but when 12+log(O/H) exceeds 8.3, secondary N production occurs, increasing at a faster rate than O (Henry et al. 2000). The N/O ratios in the present SGRB sample span a factor ≤30 at a nearly constant redshift $z \sim 0.4$.

At present, NGC 4993 is the only SGRB located within the AGN-LINER region at a redshift close to local. We have found that – compared with LGRB and SGRB hosts (Contini 2016a) – the most significant characteristic of NGC 4993 is the power-law radiation source (AGN) and the abnormally high underlying stellar radiation flux in the IR. The amount of data for SGRB host galaxies do not allow us to look on NGC 4993 as an isolated case and to decide whether the AGN and the high N/O abundance ratios are related to the SGRB or to the high age of the galaxy. For the other SGRB host galaxies, we have used SB-dominated models to reproduce the line ratios because they are well-fitting and generally suggested by the observers. However, the observed

lines are few and the continuum SED is limited to the IR range for most of the objects. The fit of the SED leads to results similar to those obtained for active galaxies in general (AGN, SB, etc.). More data for both line and continuum spectra may reveal an AGN also within the other SGRB hosts.

*Acknowledgements.* I am very grateful to the referee for his or her comments, which substantially improved the presentation of the paper.

## References


Baldwin, J., Phillips, M., & Terlevich, R. 1981, PASP, 93, 5
Barthelmy, S. D., Chincarini, G., Burrows, D. N., et al. 2005, Nature, 438, 994
Bell, A. R. 1977, MNRAS, 179, 573
Berg, D. A., Skillman, E. D., Croxall, K. V., et al. 2012, ApJ, 754, 98
Berger, E. 2009, ApJ, 690, 231
Berger, E. 2013, ApJ, 765, 121
Berger, E. 2014, ARA&A, 52, 43
Berger, E., Price, P. A., Cenko, S. B., et al. 2005, Nature, 438, 988
Blanchard, P. K., Berger, E., Fong, W., et al. 2017, ApJ, 848, L22
Bloom, J. S., Kulkarni, S. R., & Djorgavski, S. G. 2002, AJ, 123, 1111
Cohen, R. D. 1983, ApJ, 273, 489
Contini, M. 1997, A&A, 323, 71
Contini, M. 2004, MNRAS, 675, 683
Contini, M. 2014, A&A, 564, A19
Contini, M. 2016a, MNRAS, 460, 3232
Contini, M. 2016b, MNRAS, 461, 2374
Contini, M. 2017a, MNRAS, 469, 3125
Contini, M. 2017b, MNRAS, 466, 2787
Contini, M. 2018, ArXiv e-prints [arXiv:1801.03312]
Contini, M., & Aldrovandi, S. M. V. 1983, A&A, 127, 15
Contini, M., & Viegas, S. M. 2001a, ApJS, 137, 75
Contini, M., & Viegas, S. M. 2001b, ApJS, 132, 211
Contini, M., & Contini, T. 2007, AN, 328, 953
Contini, M., Prieto, M. A., & Viegas, S. M. 1998a, ApJ, 505, 621
Contini, M., Prieto, M. A., & Viegas, S. M. 1998b, ApJ, 492, 511
Cucchiara, A., Prochaska, J. X., Perley, D., et al. 2013, ApJ, 777, 94
Cutri, R. M., Skrutskie, M. F.van Dyk, S., et al. 2003, 2MASS All Sky Catalog of Point Sources
D'Avanzo, P. 2015, JHEAp, 7, 73
de Ugarte Postigo, A., Thöne, C. C., Rowlinson, A., et al. 2014, A&A, 563, A62
De Voucouleurs, G., De Voucouleurs, A., Corwin Jr., H. J., et al. 1991, Third Reference Catalogue of Bright Galaxies, RC3.9 (New York: Springer)
Dopita, M. M., Shastri, P., Davies, R., et al. 2015, ApJS, 217, 12
Eichler, D., Livio, M., Piran, T., & Schramm, D. N. 1989, Nature, 340, 126
Ferland, G., Binette, L., Contini, M., et al. 1995, The Analysis of Emission Lines: A Meeting in Honor of the 70th Birthdays of D. E. Osterbrock and M. J. Seaton, Proceedings of the Space Telescope Science Institute Symposium, held in Baltimore, Maryland May 16–18, 1994, eds. R. Williams, & M. Livio (Cambridge University Press), 83
Fong, W., Berger, E., Chornock, R., et al. 2013, ApJ, 769, 56
Fox, D. B., Frail, D. A., Hurley, K. C., et al. 2005, Nature, 437, 845
Fruchter, A. S., Levan, A. J., Strolger, L., et al. 2006, Nature, 441, 463
Gallagher, J. S., Garnavich, P. M., Berling, P., et al. 2005, ApJ, 634, 210
Gehrels, N., White, N., Barthelmy, S., et al. 2004, ApJ, 611, 1005
Grevesse, N., & Sauval, A. J. 1998, Space Sci. Rev., 85, 161
Haggard, D., Nynka, M., Ruan, J. J., et al. 2017, ApJ, 848, L25
Han, X. H., Hammer, F., Liang, Y. C., et al. 2010, A&A, 514, A24
Henry, R. B. C., Edmund, M. G., Köppen, J. 2000, ApJ, 541, 660
Hunt, L. K., Palazzi, E., Michałowski, M. J., et al. 2014, A&A, 565, A112
Kann, D. A. 2011, ApJ, 734, 96
Kauffmann, G., Heckman, T. M., Tremonti, C., et al. 2003, MNRAS, 346, 1055
Kennicutt, R. C. 1998, ARA&A, 36, 189
Kewley, L., Dopita, M. M., Sutherland, R., Heisler, C., & Trevena, J. 2001, ApJ, 556, 121
Koski, A. 1978, ApJ, 223, 56
Kouvelioutou, C., Meegan, C. A., Fishman, G. J., et al. 1993, ApJ, 413, L101
Kraemer, S. B., Wu, C.-C., Crenshaw, D. M., & Harrington, J. P. 1994, ApJ, 435, 171
Krühler, T., Malesani, D., Fynbo, J. P. U., et al. 2015, A&A, 581, A125
Lambert, A., & Valentijn, E. A. 1989, The Surface Photometry Catalogue of the ESO-Uppsala, 1989 (Garching bei Munchen: ESO)
Leloudas, G., Hsiao, E. Y., Johansson, J., et al. 2015, MNRAS, 574, A61
Levan, A.J., Lyman, J. D., Tanvir, N. R., et al. 2017, ApJ, 848, 28
Maraston, C. 2005, MNRAS, 362, 799
Margutti, R., Berger, E., Fong, W., et al. 2012, ApJ, 756, 63
Marino, R. A., Rosales-Ortega, F. F., Sánchez, S. F., et al. 2013, A&A, 559, A114
Modjaz, M., Kewley, L., Kirshner, R. P., et al. 2008, AJ, 135, 1136
Niino, Y., Aoki, K., Hashimoto, T., et al. 2017, PASJ, 69, 27
Osterbrock, D. E. 1974, Astrophysics of Gaseous Nebulae (San Francisco: W.H. Freeman and Co.)
Palmese, A., Hartley, W., Tarsitano, F., et al. 2017, ApJ, 849, L34
Pan, Y.-C., Kilpatrick, C. D., Simon, J. D., et al. 2017, ApJ, 848, L30
Perley, D. A., Modjaz, M., Morgan, A. N., et al. 2012, ApJ, 758, 122
Rigby, J. R., & Rieke, G. H. 2004, ApJ, 606, 237
Rosswog, S., & Ramirez-Ruiz, E. 2003, MNRAS, 345, 1077
Sanders, N. E., Betancourt, M., Soderberg, A. M., et al. 2012, ApJ, 758, 132
Savaglio, S., Glazerbrook, K., & Le Borgne, D. 2009, ApJ, 691, 182
Selsing, J., Kröhler, T., Malesani, D., et al. 2018, A&A, 616, A48
Soderberg, A. M., Berger, E., Kasliwal, M., et al. 2006, ApJ, 650, 261
Vernet, J., Dekker, H., D'Odorico, S., et al. 2011, A&A, 536, A105
Viegas, S. M., & Contini, M. 1994, ApJ, 428, 113
Villar, V. A., Guillochon, J., Berger, E., et al. 2017, ApJ, 851, L21
Wu, Q., Feng, J., & Fan, X. 2018, ApJ, 855, 46